ISSN 1063-7761, Journal of Experimental and Theoretical Physics, 2018, Vol. 126, No. 2, pp. 255–261. © Pleiades Publishing, Inc., 2018.
Original Russian Text © O.A. Skaldin, O.S. Tarasov, Yu.I. Timirov, E.R. Basyrova, 2018, published in Zhurnal Eksperimental'noi i Teoreticheskoi Fiziki, 2018, Vol. 153, No. 2, pp. 304–312.

Mechanisms of Rotational Dynamics of Chiral Liquid Crystal Droplets in an Electric Field

O. A. Skaldin, O. S. Tarasov, Yu. I. Timirov*, and E. R. Basyrova

Institute of Molecules and Crystals Physics, Ufa Scientific Center, Russian Academy of Sciences, pr. Oktyabrya 151, Ufa, 450075 Russia

**e-mail: timirov@anrb.ru*

Received April 7, 2017

Abstract—The dynamics of the orientational structure of chiral nematic (CN) droplets in an isotropic medium in dc and ac electric fields is investigated by the polarized light microscopy technique. It is shown theoretically that the dynamics of rotational processes in these kinds of systems is determined by electroconvective processes developing due to the flexoelectric polarization associated with the initial configuration of the director field in droplets. It is established experimentally that the linear and quadratic regions of dependence of the rotational velocity of droplets on the electric field strength are explained by the above-mentioned mechanisms. Numerical simulation on the basis of the approach developed gives good agreement with experimental data.

DOI: 10.1134/S1063776118010181

1. INTRODUCTION

The study of the structure and physical properties of various types of liquid crystal (LC)-based disordered disperse systems is one of the topical problems in the field of crystal physics and physics of condensed media. Interest in these objects is motivated by the fact that LCs possess unusual, and often unique electro-optical and mechanical properties compared with traditional optical materials. Moreover, LCs in microdisperse systems contain numerous complex orientational structures, often including topological defects [1–3], which are easily controlled by the variation of constitutive parameters, boundary conditions, and external effects (electric and optical signals and mechanical, thermal, and magnetic effects). The applied aspect of the studies is of no less importance, because they open possibilities for the design of new functional composite materials based on disperse LC systems for optoelectronics, display technology, recording media, and information technologies [4–7].

At present, the structure and the properties of disperse systems representing suspensions of LC droplets in a polymer matrix [1, 5, 7–9] and in porous glasses and films [10] and LC emulsions and gels [1, 8] have been most comprehensively studied. However, in recent years, great interest has been shown in disperse systems that represent suspensions of LC droplets in an isotropic fluid [11–13]. These systems are simpler in preparation but have been less studied; therefore, the study of the properties and structural changes in (micron- and submicron-size) LC droplets under external forces seems to be an important problem.

Note that the main types of nematic LC-droplet structures and, accordingly, transitions between them, are well enough studied [2] compared with chiral systems or cholesteric LCs, in which the presence of a helically twisted supermolecular structure of a given phase determines a number of their unique properties. An example of such a medium is given by nematic cholesterol and a disperse system of droplets based on it, in which a significant role is played by boundary effects. The latter fact should initiate interesting structural–orientational transformations in droplets in electric fields: for example, cyclic processes with period much greater than the period of the effective electric field [14], and, which is quite nontrivial, rotations of droplets in a dc electric field [15]. In this relation, a detailed study of the mechanisms of rotational dynamics of weakly chiral LC droplets dispersed in an isotropic fluid in electric fields and application of adequate theoretical models to the analysis of experimental results to establish the mechanisms underlying this dynamics seem to be topical.

The first experimental observations of LC droplet dispersions in an isotropic medium were reported by Lehmann [16] as early as at the end of the 19th century. He found a wide variety of structures of various symmetries of both static and dynamic types (rotation of LC droplets) that develop in a temperature gradient field [17, 18]. The rotation of LC droplets was also observed in an electric field [19, 20]. The nature of

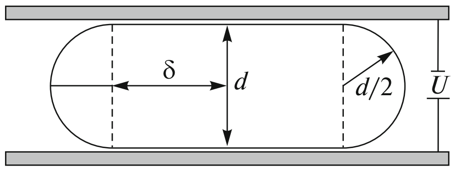

Fig. 1. Schematic view of an oblate LC droplet ($R = \delta + d/2$ is the radius of the droplet).

these phenomena was interpreted as a manifestation of thermo- and electromechanical mechanisms inherent in chiral LC systems [21, 22]. However, in [23], the authors theoretically showed that the translational motion of "cholesteric fingers" in an electric field can be initiated by electrohydrodynamic (EHD) instability with regard to the flexoelectric mechanism, which can be used to explain the rotation of droplets in a chiral nematic (CN) mixture.

Thus, in spite of the presence of theoretical models of the rotation mechanisms of LC droplets in an electric field, there is no unambiguous explanation of its physical nature. This is associated, among other things, with the lack of experimental data including the determination of the effect of the chirality of the LC medium and the size of droplets on the character of rotation. The goal of the present study is the experimental and theoretical explanation of the rotational dynamics of chiral nematic LC (CNLC) droplets in an electric field.

2. EXPERIMENTAL

As test samples, we used a mixture based on a nematic LC *n*-(4-methoxybenzylidene)-4-butylaniline (MBBA) and a cholesteric LC, cholesteryl chloride (CC), in the range from 0.05 to 2.8 wt %, so that the equilibrium helix pitch P in these mixture ranged from 238 to 4 μm. The relaxation time of induced charge in these mixtures with conductivity $\sigma \approx 2.75 \times 10^{-9}$ $(\Omega\ \mathrm{m})^{-1}$ was $\tau_q \approx 1.7 \times 10^{-2}$ s. The helix pitch of these mixtures was determined by the method described in [24]. A cell with an LC layer thickness of 25 ± 0.3 μm was placed on an HCS250 (Instec, USA) thermal table with thermal stabilization better than 0.01°C. The thickness of the samples was measured by the interference method with the use of a USB-650 (Ocean Optics Ltd., USA) optical-fiber spectrometer with an accuracy of 0.3 μm. The thermal table was mounted on a rotating object stage of an AxioImager A1 (Carl Zeiss, Germany) polarized light microscope. To obtain droplets in the isotropic environment, the LC cell was overheated so that the LC was completely transformed to the isotropic state and then slowly cooled until mesophase nuclei appear, which grew during cooling to form LC droplets of a desired size. The size of the droplets was varied by cooling or heating the cell. The electro-optical characteristics were measured in transmitted light under crossed nicols condition.

The object of study is free suspended oblate LC droplets dispersed in an isotropic melt. The droplet size was measured with the use of AxioVision (Carl Zeiss, Germany) software with built-in system for determining the size of objects. The accuracy of determination of the droplet size was about 1 μm. The experimental video image sequences obtained by a VX-440 (PCO, Germany) camera were digitized by a Pinnacle USB-700 (Pinnacle System, Germany) frame grabber with resolution of 720 × 576 pixels and recorded on a hard disk for further processing. An ac electric voltage U with frequency $f = 50$ Hz from an SFG-3015 (GW Instek, Taiwan) waveform generator with absolute error $\pm(0.05U + 0.05)$ V in the frequency range from 10 Hz to 1 MHz, or a dc electric field from a GPS-3303 (GW Instek, Taiwan) source with a discrete output voltage step of 0.01 V were applied to the LC layer.

To measure the dynamic characteristics of CNLC droplets, such as the velocity of rotation, we applied the following technique. The video record with experimental data was opened in a special video-sequence processing software with frame-by-frame scanning. To determine the rotation period, we fixed the initial position at time t_1 and, upon passing a full period of 2π, fixed the end time t_2. The ratio of the full period to the difference $T = t_2 - t_1$ determines the angular velocity of rotation $\omega = 2\pi/T$ rad/s with accuracy of Δt = 0.01 s.

3. THEORETICAL MODEL OF THE DYNAMICS OF AN OBLATE DROPLET

As a model object of study, we consider an oblate CNLC droplet in an isotropic environment placed between two infinite parallel plates (Fig. 1).

The geometry of the problem is considered in a cylindrical system of coordinates. The z axis is perpendicular to the bounding plate of the sample, i.e., along the helix axis in the central part of the droplet, and r and φ are the radial and azimuthal coordinates, respectively. The origin of the coordinate system is at the center of the droplet. The size of the CNLC droplet is determined by the radius δ and the height d of its central planar (cylindrical) part. The toroidal part of the droplet has inner radius $d/2$ and outer radius δ. A dc electric field $\mathbf{E}$ is applied along the z axis and has components $(0, 0, E)$.

To describe the physical dynamics of CNLC droplets in an isotropic medium in a dc electric field, we apply differential equations of continuum mechanics in an anisotropic fluid [21, 25, 26] with regard to the flexoelectric effect, which was considered in [23] to study the dynamics of cholesteric fingers.

In view of the complexity of the geometry of the problem and the awkwardness of the equations, analytic calculation is impossible, and we solve the problem numerically. Introduce dimensionless variables

$$r = \tilde{r}\delta, \quad z = \tilde{z}d, \quad v_{r,\varphi} = \tilde{v}_{r,\varphi}\frac{\delta}{\tau}, \\ v_z = \tilde{v}_z\frac{d}{\tau}, \quad E = \tilde{E}\frac{U_{\rm F}}{d}, \tag{1}$$

where $U_{\rm F} = \sqrt{K_{\rm el}/\varepsilon_0}$ is the voltage corresponding to the Frederiks transition, $K_{\rm el}$ is the Franck elasticity constant, $\tau = \eta d^2/K_{\rm el}$ is the relaxation time of the director, and $\eta = \alpha_4/2$ is the viscosity. Then we can write EHD equations in the same form as in [23] but with different dimensionless coefficients.

The deformation field of the director in the droplet (as shown in Fig. 2) produces volume charges, which are related to the induction of flexoelectric polarization $\mathbf{P}^{\rm fl}$; this gives rise to a force $\rho_{\rm el}\mathbf{E}$ in the Navier–Stokes equations ($\rho_{\rm el}$ is the electric charge density). In the experiments of [19, 20], the velocities on the surfaces of rotating droplets did not exceed 1 μm/s, and typical voltages were 2–4 V, which are 2–3 times less than the threshold voltage for electroconvection in LC by the Carr–Helfrich mechanism [21]. Thus, we can assume that the velocities induced in the CNLC droplets are small compared with the velocities due to electroconvection; this allows us to seek solutions to EHD equations within perturbation theory, where the small parameter is the conductivity σ:

$$\mathbf{n} = \mathbf{n}_0 + \mathbf{n}_1 + \ldots, \\ \mathbf{v} = \mathbf{v}_1 + \ldots, \\ \rho_{\rm el} = \rho_{\rm el1} + \ldots, \\ \mathbf{E} = \mathbf{E}_0 + \mathbf{E}_1 + \ldots. \tag{2}$$

Then, the Navier–Stokes equation with regard to new variables (1) has the following explicit form in cylindrical coordinates:

$$\left(\Delta v_{r1} - \frac{v_{r1}}{r^2} - \frac{2}{r^2}v_{\varphi1,_\varphi}\right)_{,z} - \varpi^2\Delta v_{z1,_r} = b^4E_0\rho_{\rm el1,_r}, \\ \left(\Delta v_{\varphi1} - \frac{v_{\varphi1}}{r^2} - \frac{2}{r^2}v_{r1,_\varphi}\right)_{,z} - \varpi^2\Delta v_{z1,_\varphi} = b^4E_0\rho_{\rm el1,_\varphi}, \tag{3}$$

where $\varpi = d/\delta$,

$$b^4 = \frac{d^4}{\delta^2\xi_{fl}\xi_F}, \quad \xi_{fl} = \sqrt{\frac{K_{\rm el}}{\varepsilon_0E_{fl}^2}}, \quad \varepsilon_F = \sqrt{\frac{K_{\rm el}}{\varepsilon_0E_F^2}}, \\ E_{fl} = \frac{e_{11}}{\varepsilon_0 d}, \quad E_F = \frac{U_F}{d}, \tag{4}$$

and e_{11} is the flexoelectric coefficient. Equations (3) are supplemented with the incompressibility condition

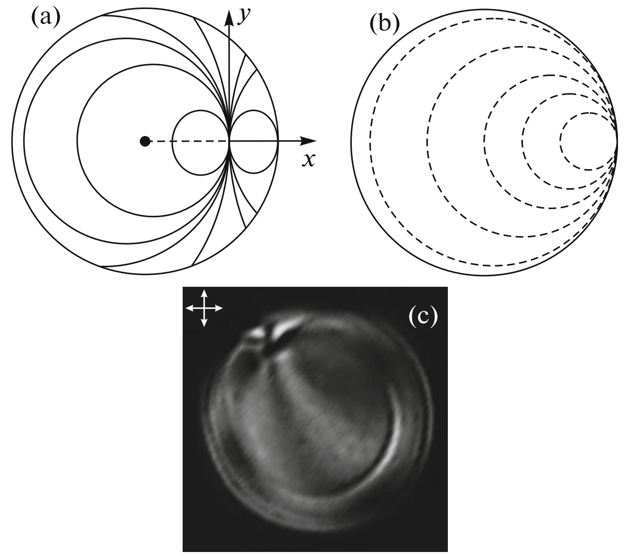

Fig. 2. (a) Model distribution of the director field in a spherical cholesteric LC droplet (the Franck–Price model). (b) Monopolar structure of a droplet with a point defect on the surface, corresponding to the distribution of the director in the plane of the section passing through the center of the cholesteric LC droplet. (c) View of an CNLC droplet with a helix pitch of $P = 54$ μm (the droplet radius is $R \approx 50$ μm) under crossed Nicol prisms.

$$\frac{1}{r}(rv_{r1})_{,r} + \frac{1}{r}v_{\varphi1,_\varphi} = v_{z1,_z} = 0. \tag{5}$$

The expression for the electric charge density has the form

$$\rho_{\rm el} = e_{fl}\nabla\cdot\left\{\mathbf{n}_0(\nabla\cdot\mathbf{n}_0) + \frac{e_3}{e_1}(\mathbf{n}_0\cdot\nabla)\mathbf{n}_0\right\}. \tag{6}$$

This expression lacks the frequency-dependent part of flexoelectric charge density [23], which is proportional to $(1 + \omega^2\tau_q^2)^{-1}$. In the general case, one can theoretically show that the frequency-dependent part of this expression can be neglected irrespective of the experimental conditions [27], especially as $\omega^2\tau_q^2 \gg 1$ for the voltage frequency $f \approx 50$ Hz considered in this paper. The theory stated in [23] can well be applied for relaxation times of $\tau_q = \varepsilon_0\varepsilon_\perp/\sigma_\perp \approx 10^{-3}$ and higher ($\sigma_\perp$ and $\varepsilon_\perp$ are perpendicular components of electric conductivity and dielectric permittivity). However, for $\tau_q \ll 10^{-3}$, this approximation is not valid for two reasons. First, the perturbation theory in which the system of equations is solved involves, as a small expansion parameter, the conductivity σ of the medium, and, second, the approach developed in [23] and, accordingly, in the present study, is based on a bipolar electrodiffusion model for electroconvection in nematics [28], which is naturally restricted by ion relaxation times related to the charge mobility.

The inhomogeneous linear equations (3) and (5) for $\mathbf{v}_1$ depend on the static distribution of the CNLC droplet director and have the following general solution [23]:

$$\mathbf{v}_1 = b^4 E_0 \mathbf{f}_1 + b^4 \xi_H E_0^2 \mathbf{f}_2, \quad (7)$$

where $\xi_H = \sigma_a/\sigma_\perp - \varepsilon_a/\varepsilon_\perp$ is the Helfrich parameter for MBBA ($\xi_H = 0.1$–0.5), σ_a and ε_a are the anisotropies of these quantities, the function $\mathbf{f}_1$ depends only on the static distribution of the CNLC droplet director and the flexoelectric coefficient, and $\mathbf{f}_2$ depends also on the ratio e_3/e_1 of flexoelectric coefficients.

The static configuration of the director in a droplet can, in principle, be obtained by solving the zero-order equation for the director field, which is a complicated problem. Therefore, instead, we apply an approximate analytic model. The first-order equation for the director field has the following form [23]:

$$\begin{aligned} &\underline{\underline{\delta_0^\perp}}\mathbf{h}_1^r + \underline{\underline{\delta_1^\perp}}\mathbf{h}_0^r = (\omega\partial_\varphi + \mathbf{v}_1 \cdot \nabla)\mathbf{n}_0 \\ &-\mathbf{\Omega}_1 \times \mathbf{n}_0 + \gamma_2 \underline{\underline{\delta_0^\perp A_1}}\mathbf{n}_0, \end{aligned} \quad (8)$$

where $\mathbf{v}_1$ is the perturbation velocity; $\gamma_2 = \alpha_6 - \alpha_5$ is the coefficient of rotational viscosity; $\mathbf{h}_0^r$ and $\underline{\underline{\delta_0^\perp}}$ include only $\mathbf{n}_0$, while $\underline{\underline{\delta_1^\perp}}$ depend on the perturbed director $\mathbf{n}_1$; $\mathbf{\Omega}_1 = \nabla \times \mathbf{v}_1/2$ is the velocity of local rotation of the fluid, and $\underline{\underline{A_1}} = \nabla \cdot \mathbf{v}_1/2$ is the hydrodynamic stress tensor. Underlined characters are used to avoid pile-up of indices; for example, $A_{1_{i,j}} \equiv \underline{\underline{A_1}}$.

In the homogeneous case, Eq. (8) takes the form

$$\underline{\underline{\delta_0^\perp}}\mathbf{h}_1^r + \underline{\underline{\delta_1^\perp}}\mathbf{h}_0^r = 0 \quad (9)$$

and has a solution corresponding to the rotation of the director. The linear operator in Eq. (9) is self-adjoint. The condition of nontrivial solvability of Eq. (8),

$$\begin{aligned} &\Big\langle \frac{\partial \mathbf{n}_0}{\partial \varphi} \cdot [(\omega\partial_\varphi + \mathbf{v}_1 \cdot \nabla)]\mathbf{n}_0 \\ &-\mathbf{\Omega}_1 \times \mathbf{n}_0 + \gamma_2 \underline{\underline{\delta_0^\perp A_1}}\mathbf{n}_0] \Big\rangle = 0, \end{aligned} \quad (10)$$

yields an expression for the rotation velocity ω:

$$\omega = b^4 E_0 \frac{I_1}{I_0 + I_2} + b^4 \xi_H E_0^2 \frac{I_3}{I_0 + I_2}, \quad (11)$$

where

$$\begin{aligned} I_0 &= \langle \mathbf{n}_{0,\varphi} \cdot \mathbf{n}_{0,\varphi} \rangle, \quad I_1 = \langle \mathbf{n}_{0,\varphi} \cdot \mathbf{g}_1 \rangle, \\ I_2 &= \langle \mathbf{n}_{0,\varphi} \cdot \mathbf{g}_2 \rangle, \quad I_3 = \langle \mathbf{n}_{0,\varphi} \cdot \mathbf{g}_3 \rangle. \end{aligned} \quad (12)$$

The integrals (12) are calculated numerically provided that the distribution of the director $\mathbf{n}_0$ and its derivatives is known; the functions $\mathbf{g}_i$ are expressed algebraically in terms of $\mathbf{f}_i$ by the substitution of expression (7) into (10), the functions $\mathbf{f}_i$ are determined by the numerical solution of Eqs. (3) and (5), and the scalar product is defined as $\langle \mathbf{a} \cdot \mathbf{b} \rangle = \iiint (\mathbf{a} \cdot \mathbf{b}) r dr d\varphi dz$.

For an appropriate basic configuration of the director, the EHD model allows one to calculate numerically the rotation velocity of the CNLC droplet in an electric field.

The numerical calculation of the director field distribution in the CNLC droplet in a three-dimensional model presents a nontrivial problem. The main difficulty is due to the presence of defects, which require the use of a tensor order parameter; this leads to a significant increase in the number of equations. On the other hand, there exist approximate analytic models that describe the distribution of the director in nematic and cholesteric droplets incorporated into various media, for example, into a polymeric matrix. In the present study, we apply the director field model considered in [29] for a spherical cholesteric LC droplet in a dc electric field. In this case, the director distribution in the central part of the droplet has the form

$$\begin{aligned} \mathbf{n} = &\frac{\rho_N^2 \cos(\varphi + qz) - \cos(\varphi - qz) + 2\rho_N \sin(qz)}{1 + \rho_N^2 - 2\rho_N \sin\varphi} \cdot \mathbf{e}_r \\ &+ \frac{\rho_N^2 \sin(\varphi + qz) + \sin(\varphi - qz) - 2\rho_N \cos(qz)}{1 + \rho_N^2 - 2\rho_N \sin\varphi} \cdot \mathbf{e}_\varphi, \end{aligned} \quad (13)$$

where $\rho_N = r\eta(z)$, $\eta(z) \equiv 2/(2 + \varpi\pi|z|)$ and $q = 2\pi/P$ is the wave vector of the cholesteric helix.

To simplify the problem and reduce technical requirements, below we consider only the central part of the droplet. This means that we have to solve Eqs. (3) and (5) in a cylinder of height d and radius δ.

The linearized Navier–Stokes equations (3), combined with the incompressibility condition (5), are solved by the Galerkin method [30]; i.e., the velocity components are expressed as follows:

$$v_{s1} = \sum_{i=1}^{N_r} \sum_{j=1}^{N_\varphi} \sum_{k=1}^{N_z} a_{ijk}^s f_i^s(r) g_j^s(\varphi) p_k^s(z), \quad s = r, \varphi, z, \quad (14)$$

where $f_i^s(r)$, $g_j^s(\varphi)$, and $f_k^s(z)$ are test functions.

The boundary conditions for the velocity are chosen so that the velocity vanishes on the surface of the cylinder: $\mathbf{v}_1 = 0$ for $z = \pm 1/2$ and $r = 1$. Then the corresponding test functions have the form

$$\begin{aligned} f_i^s(r) &= T_{i-1}(2r - 1), \\ p_k^s(z) &= \begin{cases} \cos(k\pi z), & k = 1, 3, 5, \ldots, \\ \sin(k\pi z), & k = 2, 4, 6, \ldots, \end{cases} \end{aligned} \quad (15)$$

where $s = r$, φ, z and T_i are Chebyshev polynomials. In the azimuthal direction, the velocity is expanded in a Fourier series:

$$g_j^{r,\varphi,z}(\varphi) = \begin{cases} \sin([j+1]/2\varphi), & j = 1,3,5,\ldots, \\ \cos(j/2\varphi), & j = 2,4,6,\ldots. \end{cases} \quad (16)$$

Moreover, due to the specificity of the cylindrical system of coordinates, one should use the following conditions at the origin [29]:

$$\left.\frac{\partial \mathbf{v}_1}{\partial \varphi}\right|_{r=0} = 0, \quad (17)$$

or (in components),

$$\begin{aligned} v_{r1,_\varphi} - v_{\varphi 1} &= 0, \\ v_{r1} + v_{\varphi 1,_\varphi} &= 0, \\ v_{z1,_\varphi} &= 0. \end{aligned} \quad (18)$$

Substituting expansion (14) into Eqs. (3) and (5) and using the test functions (15) and (16), we obtain an inhomogeneous system of linear algebraic equations. Then, solving Eq. (10), we find the rotation velocity ω of the droplet (11).

The main source of numerical errors is the choice of parameter values in N_r, N_φ, and N_z in the Galerkin approximation method (14), which in the present case gives a relative error of 20%. The calculations were performed for $N_r = N_\varphi = N_z = 5$ with the following constitutive parameters:

$$\delta = 15 \times 10^{-6}\ \text{m}, \quad d = 25 \times 10^{-6}\ \text{m}, \quad U_F = 0.75\ \text{V},$$

$$K_{\text{el}} = 5 \times 10^{-12}\ \text{N}, \quad \alpha_4 = 82.6 \times 10^{-3}\ \text{N s/m}^2,$$

$$e_{11} = -9.5 \times 10^{-12}\ \text{C/m}, \quad e_{33} = -13.5 \times 10^{-12}\ \text{C/m},$$

$$e_{\text{fl}} = -17.19 \times 10^{-12}\ \text{C/m}, \ \sigma_a = 1.27 \times 10^{-7}\ (\Omega\ \text{m})^{-1},$$

$$\sigma_\perp = 2.75 \times 10^{-7}\ (\Omega\ \text{m})^{-1}, \ \varepsilon_a = -0.53, \text{and } \varepsilon_\perp = 5.4.$$

Thus, according to expressions (7) and (11), the electric-field dependence of the angular velocity of rotation of droplets contains both linear and quadratic terms, and their factors contain flexocoefficients. Note that both contributions are of EHD nature, and the numerical ratio between linear and quadratic contributions is $\xi_H^{-1} \approx 5$; i.e., at low voltages, the quadratic term can be neglected.

4. COMPARATIVE ANALYSIS OF EXPERIMENTAL RESULTS WITH NUMERICAL CALCULATIONS

The determination of the rotation mechanisms of dispersed droplets in an electric field is a complicated problem because this process may involve several mechanisms: electromechanical and electroconvective with regard to the flexoeffect. The first, hypothetic case, is based on the representation of the relation between the rotation angle φ of the director and the external electric field E in terms of the so-called electromechanical coefficient ν_e:

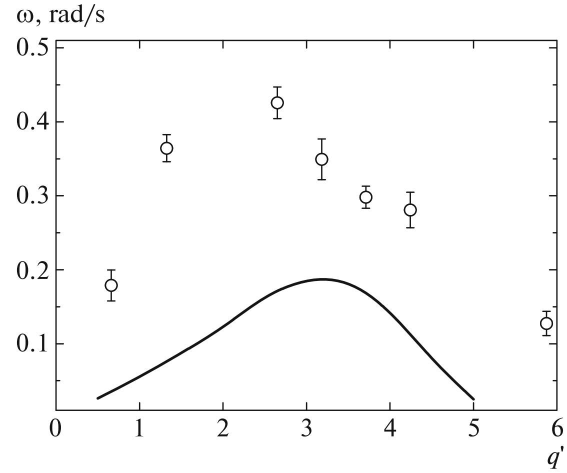

Fig. 3. Experimental and calculated angular velocity of rotation of CNLC droplets as a function of the reduced wave vector $q' = q/q_0$, where $q = 2\pi/P$ is the wave vector of the helical structure of an CNLC droplet defined by cholesteric dopants and $q_0 = 2\pi/d$. The solid curve corresponds to calculated data.

$$\varphi = q_0 z + \frac{\nu_e E t}{\gamma_1},$$

where q_0 is the wave vector of the chiral mixture and γ_1 is the viscosity. Hence, for the angular rotation velocity we obtain

$$\omega = \frac{\partial \varphi}{\partial t} = \frac{\nu_e E}{\gamma_1}.$$

This expression implies that the rotation velocity of the director linearly depends on the applied voltage and is independent either of the droplet size or the value of the wave vector. This is an important point for solving the problem of rotation of LC droplets in an electric field.

Let us show that the rotation of CNLC droplets in a dc electric field, which was interpreted by the authors of [19, 20] as a manifestation of the electromechanical effect, can be explained within the EHD approach based on the dynamics of induced charges in the director field deformed due to the flexoelectric polarization. To this end, we analyze the angular rotation velocity as a function of applied dc electric voltage, the wave vector q of the helical structure of droplets, and the size R of the droplets.

First, according to the theory, the rotation velocity of droplets changes its sign depending on the value of the wave vector q of the helix. For left-twisted chiral LCs, the droplets rotate clockwise (as seen along the direction of the field **E**, i.e., $\omega > 0$), while, for right-twisted LCs, the droplets rotate counterclockwise, $\omega < 0$. The CNLC droplets considered in this study are left-twisted LCs; hence, $\omega > 0$, which is confirmed by the results obtained (Fig. 3). Moreover, the results of the numerical calculation of the angular velocity of

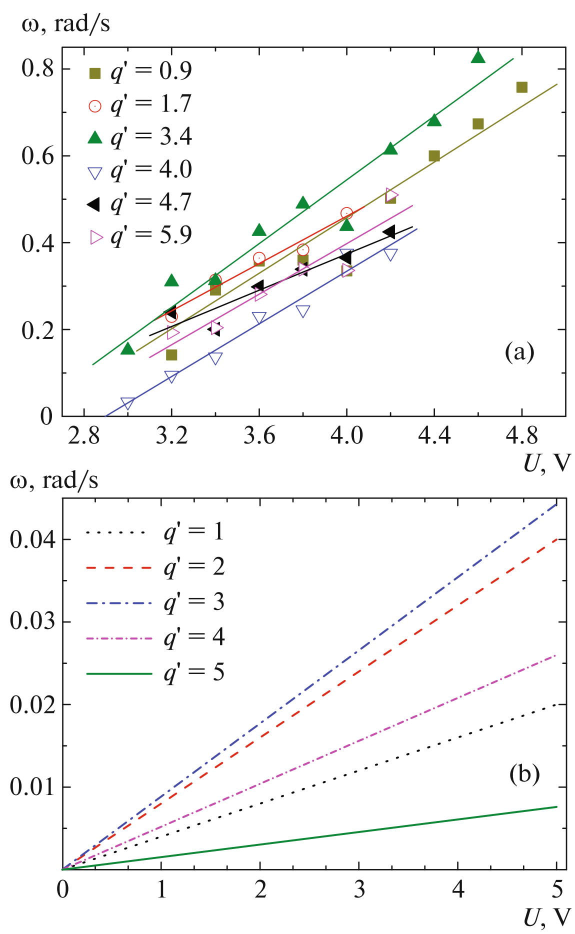

Fig. 4. (Color online) (a) Experimental and (b) calculated angular velocity ω of rotation of CNLC droplets as a function of the applied voltage U for various values of q'.

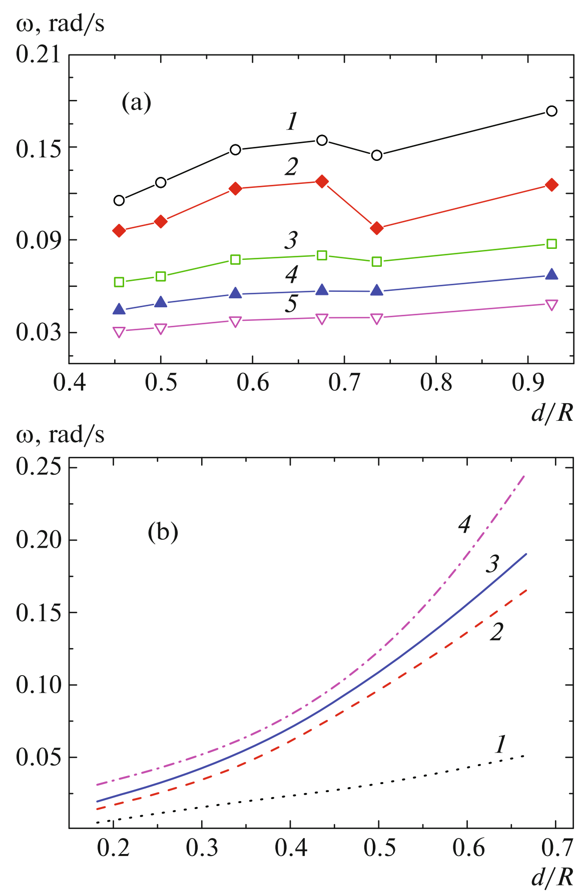

Fig. 5. (Color online) Angular velocity of rotation of CNLC droplets as a function of d/R; (a) experimental curves plotted for voltage values of U = 4.5 (*1*), 4.0 (*2*), 3.3 (*3*), 2.8 (*4*), and 2.4 V (*5*); (b) calculated data for voltage values of U = 1 (*1*), 2 (*2*), 3 (*3*), and 4 V (*4*).

rotation as a function of the wave vector q of the helix in a droplet (Fig. 3) are in sufficiently good agreement with the experimental dependence (Fig. 3).

Second, the experimental dependence of the angular velocity of rotation of a droplet linearly depends on the electric field (Fig. 4a), which qualitatively agrees with the results of numerical calculation (Fig. 4b) and corresponds to the first term in expression (11), which is related to the flexoelectric effect.

Third, we also obtained experimental dependence of the angular velocity of rotation of droplets on their radius (Fig. 5a), which is in good agreement with the calculated data (Fig. 5b). Here we should also note that there is no such dependence on the droplet size within the electromechanical coupling mechanism [20].

5. CONCLUSIONS

Thus, the observed effect seems to be based on the EHD instability, which develops due to the presence of bound flexoelectric charges induced by the strong deformation of the orientation field of the director in the bulk of a droplet, especially near the defects; this conclusion is based on three experimental results (see Figs. 3, 4, and 5a), which are in good agreement with numerical results (see Figs. 3, 4b, and 5b).

As regards the reduction in the electroconvection threshold, this is associated, in our opinion, with the fact that the equilibrium structure of a droplet—bent cholesteric planes—guarantees the presence of charge sink regions (of both positive and negative signs) at arbitrarily small voltages; i.e., it is as if the elastic component is subtracted from the expression for the threshold value of the EHD convection field. A similar behavior is observed in the so-called cholesteric fingers—complex structures that arise near the nematic–cholesteric transition region [23]. Cholesteric fingers move translationally in an electric field (either dc or ac field, depending on the symmetry of the orientation field of cholesteric fingers) at voltages much lower than the EHD-instability voltage.

It is also important that, under scrupulous examination, the mechanisms discussed in this paper show a certain similarity with the mechanism of EHD instability in the isotropic phase, which accompanies electroconvection in anisotropic droplets formed in the bulk of a chiral nematic sample. The last fact is confirmed by the convective motion of microparticles. However, the fundamental feature of the effect is that the rotation of the axis of the cholesteric phase in an anisotropic droplet is insensitive to a change in the sign of the applied electric field. This is indicative of the fact that the moments of forces causing the rotation of a droplet contain even powers of electric-field strength, as is characteristic of the EHD effect, which is quadratic in electric field.

Moreover, we should note that the rotation velocity of a droplet essentially depends on the twist wave vector q, i.e., on the cholesteric concentration (see Figs. 4 and 5), the maximum being attained for $q \sim q_0$. This dependence also points to the EHD nature of the rotation of droplets, because the moments of forces acting on the LC from the electric field in the Carr–Helfrich mechanism are quadratic in the gradients of the orientation field, and viscous moments, with regard to the fluid velocity gradients, contain higher degrees of such gradients. Therefore, for stronger twists of the LC, the rotation of droplets is suppressed by viscosity, whereas, for weak twists, the effect of the cholesteric component of the LC is eliminated.

ACKNOWLEDGMENTS

We are grateful to A.P. Krekhov for useful recommendations and discussions.

This work was supported in part by the Russian Foundation for Basic Research (project no. 15-02-09366) and by a grant of the President of the Russian Federation (project no. SP-183.2016.1). Experimental investigations were carried out with the use of the equipment of TsKP Spectr IFCP URC RAS and RTsKP Agidel'.

REFERENCES

1. G. P. Crawford and S. Zumer, *Liquid Crystals in Complex Geometries* (Taylor and Francis, London, 1996).
2. G. E. Volovik and O. D. Lavrentovich, Sov. Phys. JETP **58**, 1159 (1983).
3. M. V. Kurik and O. D. Lavrentovich, Sov. Phys. Usp. **31**, 196 (1988).
4. H. G. Graighead, J. Cheng, and S. Hackwood, Appl. Phys. Lett. **40**, 22 (1982).
5. G. M. Zharkova and A. C. Sonin, *Liquid Crystal Composites* (Nauka, Novosibirsk, 1994) [in Russian].
6. P. S. Drzaic, *Liquid Crystal Dispersions* (World Scientific, Singapore, 1995).
7. J. W. Doane, A. Golemme, J. L. West, J. B. Whitehead, and B. G. Wu, Mol. Cryst. Liq. Cryst. **165**, 511 (1988).
8. S. J. Klosowicz and J. Zmija, Opt. Eng. **34**, 3440 (1995).
9. O. O. Prishchepa, A. V. Shabanov, V. Ya. Zyryanov, A. M. Parshin, and V. G. Nazarov, JETP Lett. **84**, 607 (2007).
10. D. Semerenko, D. Smeliova, S. Pasechnik, A. Murauskii, V. Tsvetkov, and V. Chigrinov, Opt. Lett. **35**, 2155 (2010).
11. Yu. I. Timirov, O. S. Tarasov, and O. A. Skaldin, Tech. Phys. Lett. **33**, 209 (2007).
12. O. A. Skaldin and Yu. I. Timirov, JETP Lett. **90**, 633 (2009).
13. G. I. Maksimochkin, S. V. Pasechnik, and A. V. Lukin, Tech. Phys. Lett. **41**, 676 (2015).
14. Yu. I. Timirov, O. A. Skaldin, E. R. Basyrova, and Yu. A. Lebedev, Phys. Solid State **57**, 1912 (2015).
15. Yu. I. Timirov, O. A. Skaldin, and E. R. Basyrova, Tech. Phys. Lett. **41**, 336 (2015).
16. O. Lehmann, Ann. Phys. **2**, 649 (1900).
17. P. Oswald and A. Dequidt, Phys. Rev. Lett. **100**, 217802 (2008).
18. T. Yamamoto, M. Kuroda, and M. Sano, Europhys. Lett. **109**, 46001 (2015).
19. N. V. Madhusudana and R. Pratibha, Liq. Cryst. **5**, 1827 (1989).
20. N. V. Madhusudana, R. Pratibha, and H. P. Padmini, Mol. Cryst. Liq. Cryst. **202**, 35 (1991).
21. P. G. de Gennes and J. Prost, *The Physics of Liquid Crystals* (Clarendon, Oxford, 1993).
22. N. V. Madhusudana, in *Modern Topics in Liquid Crystals*, Ed. by A. Buka (World Scientific, Singapore, 1989), p. 195.
23. O. S. Tarasov, A. P. Krekhov, and L. Kramer, Phys. Rev. E **68**, 031708 (2003).
24. O. A. Skaldin, Yu. I. Timirov, and Yu. A. Lebedev, Tech. Phys. Lett. **36**, 885 (2010).
25. S. A. Pikin, *Structural Transformations in Liquid Crystals* (Nauka, Moscow, 1981; Gordon and Breach Sci., New York, 1991).
26. L. D. Landau and E. M. Lifshitz, *Course of Theoretical Physics*, Vol. 8: *Electrodynamics of Continuous Media* (Nauka, Moscow, 1982; Pergamon, New York, 1984).
27. O. S. Tarasov, PhD Thesis (Univ. Bayreuth, 2003).
28. M. Treiber and L. Kramer, Mol. Cryst. Liq. Cryst. **261**, 311 (1995).
29. J. Bajc and S. Zumer, Phys. Rev. E **55**, 2925 (1997).
30. D. Gottlieb and S. A. Orszag, *Numerical Analysis of Spectral Methods: Theory and Applications* (CapitalCity, Montpelier, 1993).

Translated by I. Nikitin